Bulk-Processed Pd Nanocube-Poly(methyl methacrylate) Nanocomposites as Plasmonic Plastics for Hydrogen Sensing

(article starts on next page)

Article

Bulk-Processed Pd Nanocube−Poly(methyl methacrylate) Nanocomposites as Plasmonic Plastics for Hydrogen Sensing

Iwan Darmadi,[#] Alicja Stolaś,[#] Ida Östergren,[#] Barbara Berke, Ferry Anggoro Ardy Nugroho, Matteo Minelli, Sarah Lerch, Irem Tanyeli, Anja Lund, Olof Andersson, Vladimir P. Zhdanov, Marianne Liebi, Kasper Moth-Poulsen,* Christian Müller,* and Christoph Langhammer*

Cite This: *ACS Appl. Nano Mater.* 2020, 3, 8438−8445

Read Online

ACCESS | Metrics & More | Article Recommendations | SI Supporting Information

ABSTRACT: Nanoplasmonic hydrogen sensors are predicted to play a key role in safety systems of the emerging hydrogen economy. Pd nanoparticles are the active material of choice for sensor prototype development due to their ability to form a hydride at ambient conditions, which creates the optical contrast. Here, we introduce plasmonic hydrogen sensors made from a thermoplastic nanocomposite material, that is, a bulk material that can be molded with standard plastic processing techniques, such as extrusion and three-dimensional (3D) printing, while at the same time being functionalized at the nanoscale. Specifically, our plasmonic plastic is composed of hydrogen-sensitive and plasmonically active Pd nanocubes mixed with a poly(methyl methacrylate) matrix, and we optimize it by character-ization from the atomic to the macroscopic level. We demonstrate melt-processed deactivation-resistant plasmonic hydrogen sensors, which retain full functionality even after 50 weeks. From a wider perspective, we advertise plasmonic plastic nanocomposite materials for application in a multitude of active plasmonic technologies since they provide efficient scalable processing and almost endless functional material design opportunities *via* tailored polymer−colloidal nanocrystal combinations.

KEYWORDS: plasmonic nanocomposites, nanoparticles, polymer matrix, melt processing, 3D printing, plasmonic hydrogen sensing
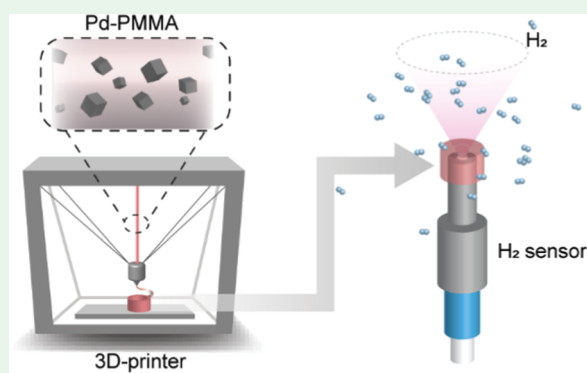

■ INTRODUCTION

Nanoparticles supporting localized surface plasmon resonance (LSPR) enable a wide range of fascinating technologies, where optical bio- and chemosensors[1−6] are of particular interest, and where hydrogen sensors show great promise as a key technology in the emerging hydrogen economy,[6−8] since safety sensors are critical due to H_2's wide flammability range in air. In this context, optical plasmonic detection is attractive since it generates no sparks due to the passive nature of the transducer and the remote readout capability of light. In this technology, the optical contrast that signals the presence of H_2 in the environment stems from the absorption of hydrogen species into interstitial sites of metal nanoparticles. Therefore, plasmonic H_2 sensors are intrinsically highly H_2-selective.[6] Pd is the prototype-active H_2 sensing material due to its ability to dissociate H_2 gas without a sizable energy barrier at ambient conditions and its reversible phase transformation from metal to metal hydride at room temperature[9] that gives rise to a large optical contrast.[10] However, despite these advantages, the large-scale practical implementation of plasmonic sensors in commercial devices, in general, and of hydrogen sensors, in particular, is still lacking. A key reason for this situation is that nanofabrication approaches based on nanolithography and

vacuum-based thin-film material deposition methods are mostly used for the generation of nanoplasmonic sensing functions aimed at device integration. This is both costly and limits the technology to two-dimensional (2D) arrays on flat surfaces. Thus, to enable the widespread utilization of plasmonic sensors, in general, and of hydrogen sensors, in particular, new ways to make the active plasmonic materials, as well as flexible and scalable material processing routes for three-dimensional (3D) device integration, are of critical importance. For this purpose, plasmonic nanoparticles made by colloidal synthesis[11] are very attractive since they offer unrivaled possibilities for size, composition, and structural engineering to, in turn, both maximize sensitivity and optimize optical performance in plasmonic hydrogen sensors.[12,13] However, even though the self-assembly of colloidal nano-
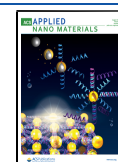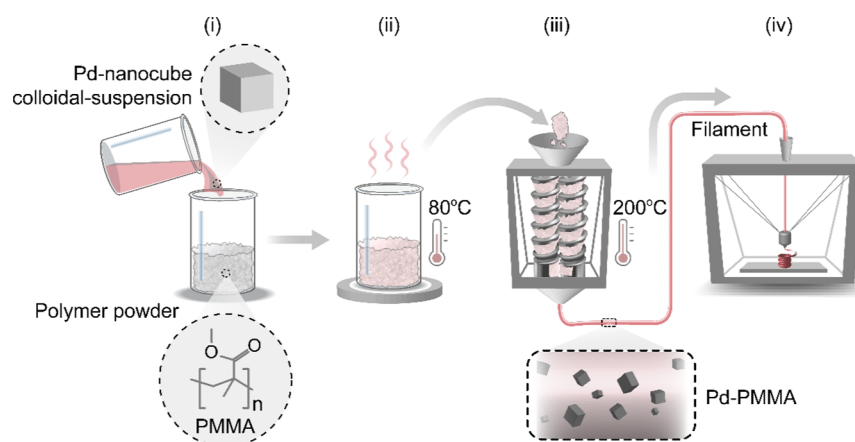
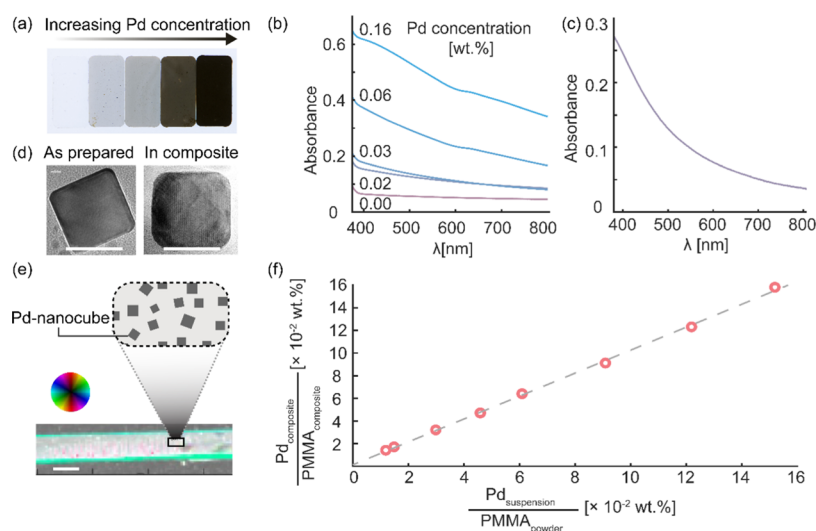**Figure 1.** Plasmonic plastic Pd−PMMA nanocomposite processing scheme. Schematic depictions of mixing, compounding, and 3D printing steps (not to scale): (i) mixing of the aqueous Pd nanocube suspension with the PMMA polymer powder; (ii) drying of the PMMA−Pd nanocube mixture; (iii) melt extrusion of the composite filament; and (iv) 3D printing of a plasmonic plastic object with hydrogen sensing function.


Figure 2. Pd nanocube−PMMA plasmonic plastic nanocomposite characterization. (a) Photograph of 500 μm thick Pd nanocube−PMMA composite plates with Pd concentrations of 0.00, 0.02, 0.03, 0.06, and 0.16 wt %. (b) Absorbance spectra of 500 μm thick Pd nanocube−PMMA nanocomposite plates with the Pd loading shown in (a). (c) Absorbance spectrum of the colloidal suspension of the as-synthesized Pd nanocubes. (d) HRTEM images of a single Pd nanocube directly after colloidal synthesis and in the PMMA matrix after compounding and melt pressing. The scale bar is 20 nm. (e) Scanning-SAXS image of a melt-pressed Pd nanocube−PMMA plate cross section with a 0.02 wt % Pd nanocube concentration. The scale bar is 500 μm. The green appearance of the sample edges is due to edge scattering. (f) Pd particle concentration in synthesis suspension versus the Pd concentration in Pd nanocube−PMMA plates obtained from elemental analysis. The analysis reveals a linear correlation between the Pd particle concentration in the synthesis solution and the Pd particle concentration in the melt-pressed composite.

crystals on surfaces[14−16] represents a reasonably mature approach in nanoscale processing, inherent deficiencies like nonscalability and limited adhesion call for alternative solutions for integration in sensor devices. Furthermore, hydrogen sensor deactivation due to "poisoning" by molecular species,[17] such as trace amounts of CO present in, for example, urban air,[18,19] or issues with cross-sensitivity[20] require urgent attention.

To address these challenges, we explore here the application of an inherently scalable paradigm of melt extrusion and 3D printing of plasmonic plastic nanocomposite materials, which are composed of a polymer matrix mixed with plasmonic metal nanoparticles that provide the sensing function. This approach only requires well-established and cost-effective bulk process-ing techniques to shape plasmonically active objects for device integration. However, neither plasmonic plastic nanocomposite materials as such nor their processing by, e.g., melt processing,

such as 3D printing, has so to date been considered for application in nanoplasmonic sensors in general and hydrogen sensors in particular. Therefore, as the key step beyond the state of the art, we explore here a plasmonic plastic nanocomposite material for melt-processed hydrogen sensors. As building blocks for the nanocomposite, we select colloidal Pd nanocubes as the active hydrogen sensing material due to their well-documented selective interaction with hydrogen *via* hydride formation and thus the ideal suitability as a model system to demonstrate our new concept,[3,21,22] and poly(methyl methacrylate) (PMMA) as a matrix material due to its demonstrated molecular sieving function.[7,20,23] After detailed structural characterization of the material to optimize its composition in terms of sensor performance, we demonstrate fully functional melt-processed plasmonic H_2 gas sensors that we validate in the form of a 3D-printed sensor cap compatible with fiber optics and a melt-pressed plate integrated into a
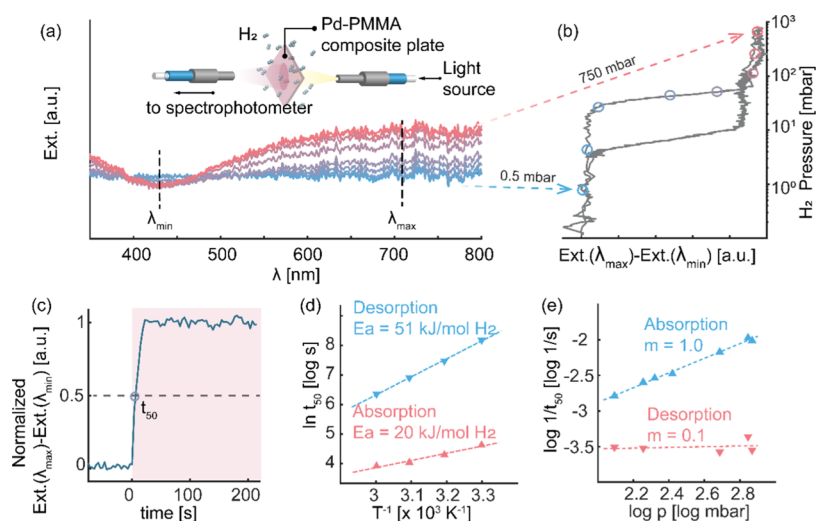
Figure 3. Pd nanocube−PMMA composite for hydrogen sensing. (a) Selected self-referenced extinction spectra evolution of a melt-pressed 50 μm thick Pd nanocube−PMMA composite plate with a 0.03 wt % Pd nanocube concentration during exposure to 0.5−750 mbar H_2 pressure at 30 °C. (b) Optical pressure−composition isotherm constructed using [extinction@λ_{max} − extinction@λ_{min}] indicated in (a) as the readout parameter with the largest optical contrast. (c) Normalized temporal [extinction@λ_{max} − extinction@λ_{min}] response upon the stepwise H_2 pressure increase from 0 to 750 mbar H_2 in the shaded area. (d) Arrhenius plot obtained from hydrogen ab/desorption kinetics measurements at different temperatures (Figure SI 4). The derived apparent activation energies, E_a, for hydrogen ab/desorption (solid up triangle/solid down triangle) are also shown. (e) Derivation of the sorption-order parameter, m, for hydrogen absorption and desorption (Figure SI 5). (c−e) were measured on a 500 μm thick Pd nanocube−PMMA composite plate.

commercial prototype sensor device. Both versions readily allow optical H_2 detection in air, as well as in a highly deactivating carbon monoxide (CO) background, and exhibit exceptional long-term stability of at least 50 weeks.

■ RESULTS AND DISCUSSION

Nanoparticle Synthesis, Composite Compounding, and 3D Printing. The first step in the process toward a functional plasmonic nanocomposite material for hydrogen sensing is the colloidal synthesis of the desired plasmonic nanocrystals. For this purpose, here, we relied on the aqueous-solution-based Pd nanocube synthesis, using hexadecyltrimethylammonium bromide (CTAB) as the stabilizing surfactant, yielding single-crystalline Pd nanocubes with a 23.2 ± 3.3 nm average side length. In the next step, the nanoparticle dispersion was mixed with the PMMA powder and then dried for 16 h at elevated temperature to evaporate the aqueous solvent (Figure 1). Hence, the mixing ratio of Pd colloidal nanoparticles and polymer powder determines the colloid concentration in the final composite. Subsequently, the nanoparticle−polymer mixture was compounded in a twin-screw microcompounder and extruded into a Pd nanoparticle−PMMA matrix composite filament of the desired dimension. This filament then served as the raw material for further processing of the composite into macroscopic plasmonic objects by melt pressing or 3D printing.

Pd Nanocube−PMMA Plasmonic Plastic Nanocomposite Characterization. As the active material for hydrogen detection, we have compounded Pd nanocube−PMMA composites with five different Pd nanocube loadings (0, 0.02, 0.03, 0.06, and 0.16 wt %) and melt-pressed the extruded filaments into 500 μm thick plates that exhibit increasingly darker coloring for increasing nanoparticle loading (Figure 2a). The grayish appearance is in good agreement with an LSPR resonance peak in the UV spectral range and the broad-band spectral absorbance of Pd nanoparticles due to interband

damping of the LSPR[24,25] both in the composite (Figure 2b) and in a colloidal suspension (Figure 2c). Furthermore, the inspection of high-resolution transmission electron microscopy (HRTEM) images of the Pd nanocubes before (in colloidal suspension) and after compounding (inside the polymer matrix) reveals the general cubic shape preservation (with an indication of slight edge-rounding) and their single-crystalline nature (Figures 2d and SI 1). Scanning-SAXS analysis of the composite with a 0.02 wt % Pd nanocube concentration in the q-range of 0.006−0.55 Å^{-1} shows a homogeneous distribution and isotropic arrangement throughout the cross-sectional slice (Figure 2e, minor segregation is observed; see Figure SI 2a−c), and also corroborates the anticipated average size of about 28.0 ± 1.8 nm of the Pd nanocubes in the composite (Figure SI 2d and Table SI 1). Finally, elemental analysis reveals that the weight ratio of the Pd nanocubes in the synthesis suspension to the PMMA powder scales linearly with the weight ratio of the Pd to the PMMA in the Pd nanocube−PMMA nanocomposite (Figure 2f). Moreover, the elemental analysis also implies that no Pd is lost during the processing.

Pd Nanocube−PMMA Nanocomposites for Plasmonic Hydrogen Detection. For the first global characterization of the Pd nanocube−PMMA nanocomposite interaction with H_2 and its corresponding optical response, we melt-pressed a 50 μm thick plate with a 0.03 wt % Pd nanocube loading. Using a vacuum chamber setup with optical windows,[26] we then measured the wavelength-resolved self-referenced (with respect to the first measured spectrum of the experiment) optical extinction of the composite for increasing H_2 gas pressure (Figure 3a). We focus on the wavelength range corresponding to the flank of the plasmonic "peak", which has been shown to yield the highest sensitivity.[26,27] The selected spectra reveal the corresponding distinct optical contrast of the composite. Continuous monitoring of the extinction difference at two selected wavelengths, λ_{min} and λ_{max}, thus enables the optical mapping of a pressure−composition isotherm of the

material due to the linear dependence of the Pd plasmonic response to H_2[10,28,29] (Figure 3b). The obtained isotherm is in excellent agreement with other studies of Pd nanocube–H_2 interactions and exhibits the characteristic low-pressure α-phase, the $\alpha + \beta$-phase coexistence plateau, and the high-pressure β-phase regions, as well as distinct hysteresis between absorption and desorption in the two-phase region.[3,21,22] This corroborates that the intrinsic material properties of the Pd nanocrystals are preserved in the nanocomposite, guaranteeing the anticipated functionality (for the corresponding analysis of neat Pd nanocubes, see Figure SI 3a,b). At the same time, this Pd-specific characteristic response to H_2 exposure has implications for sensor performance. As apparent from the measured isotherm, the most significant optical contrast change occurs at the $\alpha + \beta$-phase coexistence plateau, while it is very small in the α-phase region. This means that the material in its current form, and as characteristic for most H_2 sensors based on pure Pd, is most useful when applied for the detection of a critical H_2 threshold pressure corresponding to the two-phase coexistence plateau. To resolve this limitation and thereby significantly improve sensor detection limit, as well as to eliminate hysteresis, alloying of Pd with, e.g., Au[26] or Cu[17] has proven very effective, and we thus propose this approach also for next-generation plasmonic plastics-based hydrogen sensors.

To quantify the kinetics of hydrogen sorption in the Pd nanocube–PMMA composite, we measured the temporal response to stepwise H_2 exposure and used t_{50}, that is, the response time to 50% of the maximal steady-state signal at the new pressure (Figure 3c), as the descriptor. As the corresponding Arrhenius analysis reveals, we find apparent activation energies of 20 and 51 kJ/mol H_2 for hydrogen absorption and desorption in the composite, respectively (Figures 3d and SI 4, and Section SI 5), which is within the range of reported literature values for the Pd–H system.[7,30] Furthermore, analysis of the pressure dependence yields an order parameter, $m = 1$, for absorption and $m = 0.1$ for desorption (Figures 3e and SI 5), indicating pressure independence in the latter case.

Having established a fundamental mechanistic understanding of the Pd nanocube–PMMA nanocomposite–H_2 interaction, it is now interesting to investigate the impact of nanocomposite design parameters on H_2 sensing performance. We prepared a series of melt-pressed plates with (i) different Pd nanocube loadings (0.02–0.16 wt %) at constant 250 μm thickness and (ii) different thicknesses (100–800 μm) at a constant 0.02 wt % Pd nanocube concentration. Subsequently, we measured their response to a 750 mbar H_2 pressure step (see Figures 4a,c and SI 6 and 7 for recovery). Plotting t_{50} vs nanocube concentration (Figure 4b) and vs plate thickness (Figure 4d) reveals distinct linear and quadratic dependencies, respectively. To understand these, we developed an analytical model based on propagation of a H_2 diffusion front through the composite (Figure 4e and Subsection SI 7.1). Our model suggests that the transient kinetics of hydrogen sorption in the composite depends on the balance between H_2 diffusion in the PMMA matrix and H sorption by the Pd nanocubes. Hence, we predict that the absorption time scales linearly with nanoparticle loading and shows a quadratic dependency on the plate thickness, and fit $t_{50} = k_a^{conc} C_{NP}$ (eq S16) and $t_{50} = k_a^{thick} L^2$ (eq S18) to the experimental data in Figure 4b,d, respectively. C_{NP} and L are the nanocube concentration and plate thickness, respectively. The fitting enables the extraction of k_a^{conc} and
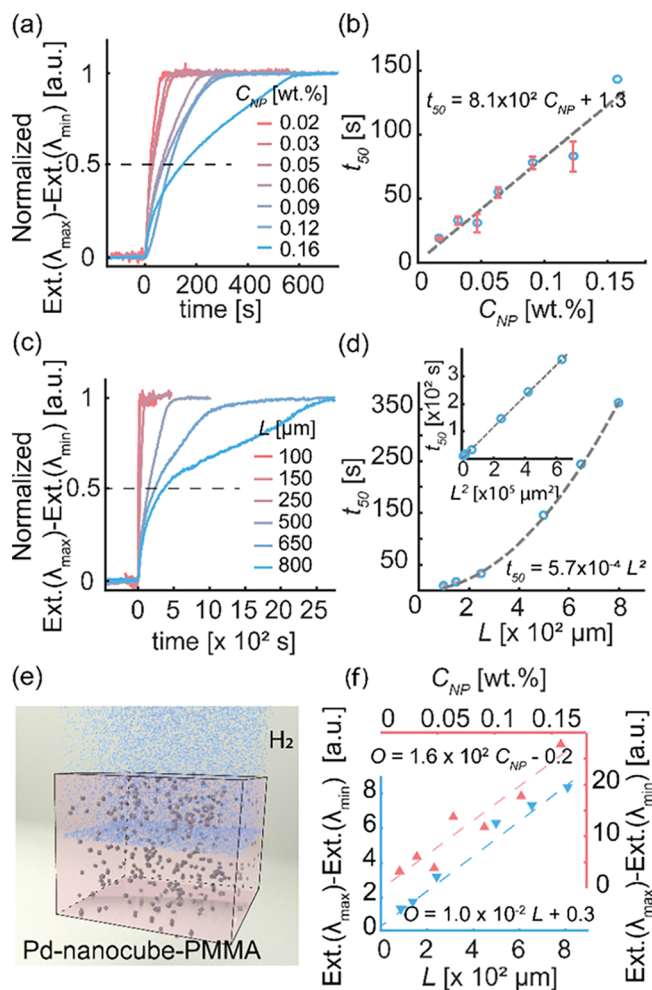
Figure 4. Hydrogen sensing kinetics and optical contrast of Pd nanocube–PMMA. (a) Normalized optical response to a stepwise H_2 pressure increase from 0 to 750 mbar at 30 °C for melt-pressed Pd nanocube–PMMA plates with different Pd loadings. (b) Temporal response (t_{50}) for the samples presented in (a) as a function of the Pd nanocube concentration in the composite. Error bars depict the standard deviation from three measurements for each sample. (c) Normalized optical response of melt-pressed Pd nanocube–PMMA plates with different thicknesses at a constant Pd nanocube concentration of 0.02 wt %. (d) Temporal response (t_{50}) for the samples presented in (c), plotted as a function of plate thickness, L, revealing a quadratic trend. The inset shows the same data plotted vs L^2. (e) Schematic mechanistic depiction of the analytical model used to analyze the experimental data. It assumes the propagation of a H_2 diffusion front. (f) Optical contrast (O) upon hydrogenation of the nanocomposite to 750 mbar H_2, defined as [extinction@λ_{max} − extinction@λ_{min}], for plates with different Pd nanocube concentrations (solid up triangle) and different thicknesses at a constant Pd nanocube concentration (solid down triangle). The dashed lines correspond to linear fits to the data.

k_a^{thick}, which are related to the H_2 diffusion constant in PMMA as

$$k_a^{conc} = c_0 V_{NP} L^2 / [64(c_f - \hat{c}_f^*) D_{conc}] \quad (1)$$

for varying Pd nanoparticle concentration, and

$$k_a^{thick} = c_0 C_{NP} V_{NP} / [64(c_f - \hat{c}_f^*) D_{thick}] \quad (2)$$

for varying plate thickness. Here, c_0 is the H concentration in the hydride, V_{NP} is the nanocube volume, c_f is the H_2

concentration in the PMMA matrix, and $\hat{c}_f^*$ is the H_2 concentration in the PMMA matrix when the nanocubes are fully hydrated. $\hat{c}_f^*$ is thus proportional to the absorption plateau pressure of Pd. The obtained diffusion constants are $D_{conc.} = 4.4 \times 10^{-7}$ cm²/s and $D_{thick} = 1.6 \times 10^{-7}$ cm²/s. These values are in good agreement with the corresponding value $D_{diff} = 6.3 \times 10^{-7}$ cm²/s obtained from direct diffusivity measurements (Figure SI 8 and Table SI 3). This means that the predominant rate-limiting factor for H_2 absorption in the nanocomposite is H_2 diffusion through the PMMA matrix and not H_2 sorption by the Pd nanocubes, in agreement with the faster response of neat Pd nanocubes (Figure SI 3c). Finally, we also quantified the optical contrast, defined as [extinction@λ_{max} − extinction@λ_{min}], between the composite in the unhydrogenated and hydrogenated states at a 750 mbar H_2 pressure (Figure 4f). Evidently, the measured optical contrast scales linearly both with increasing plate thickness at a constant Pd nanocube loading and with increasing loading at a constant thickness, in good agreement with the Beer−Lambert law.

In summary, these observations imply a trade-off between the optical contrast and temporal response for sensing. Hence, there is an optimal Pd loading and plate thickness that provides the best compromise between those two figures of merit, and we argue that it is preferable to enhance the sensing contrast by increasing the Pd loading rather than the plate thickness because the former increases the temporal response linearly, while the latter shows a quadratic dependency. Also, we predict that further tailoring of the polymer matrix in terms of H_2 permeability is a viable strategy to significantly improve the temporal response of such systems in the future.

Melt-Pressed and 3D-Printed Deactivation-Resistant Plasmonic Plastic Hydrogen Sensors. To demonstrate the ease of integration of our plasmonic plastic into real devices, we tested two different systems as deactivation-resistant H_2 sensors in the CO-rich environment:[31] (i) a melt-pressed Pd nanocube−PMMA sensor plate of 100 μm thickness with a Pd nanocube loading of 0.03 wt % and (ii) a 3D-printed Pd nanocube−PMMA sensor cap of a 200 μm effective thickness and with a 0.02 wt % Pd nanocube loading. The 200 μm thickness of the 3D-printed cap is dictated by the nozzle of the used 3D printer. To compensate for the increased thickness and its detrimental impact on response time, we have therefore reduced the Pd loading slightly, according to the design rule introduced above.

For the first test, we inserted the melt-pressed Pd nanocube−PMMA plate into a gas sensor device (Insplorion AB, Göteborg, Sweden; Figure 5a). We then exposed the sensor to subsequent cycles of 10% H_2, of 0.5% CO, and of 10% H_2 + 0.5% CO, all in the synthetic air carrier gas. Remarkably, thanks to the low diffusivity of CO in PMMA,[31] the system exhibits consistent and reliable response to H_2 even at severe CO poisoning conditions, which would readily deactivate the unprotected Pd control via strong CO chemisorption and the concurrent blocking of H_2 dissociation sites (Figure 5b).[18]

For the second test, we opted for a fiber-optic sensor solution onto which we fitted the tailor-made 3D-printed sensor cap (Figure 5c). For sensing performance testing, the cap was mounted on the tip of an SMA-terminated optical fiber mounted inside a homebuilt flow reactor using a fiber-optic feed-through (Figure SI 10c) and then exposed to subsequent cycles of 10% H_2, of 0.5% CO, and of 10% H_2 + 0.5% CO, all in the synthetic air carrier gas. Similar to the melt-
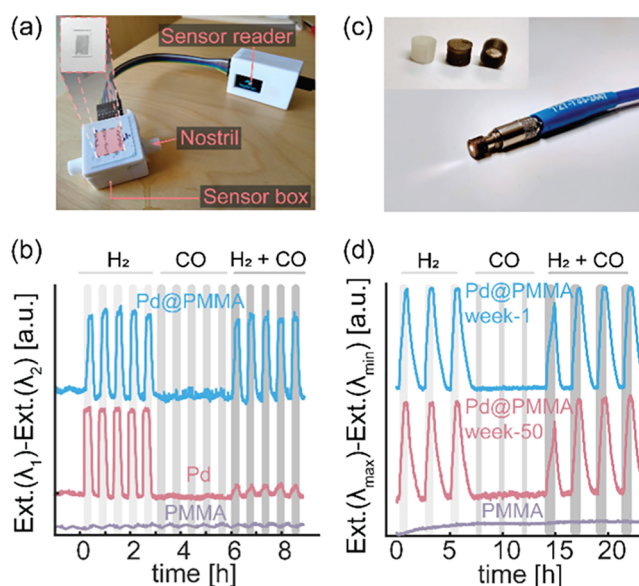
Figure 5. Device integration of melt-pressed and 3D-printed Pd nanocube−PMMA H_2 sensors. (a) Photograph of the plasmonic gas sensor prototype device provided by Insplorion AB. The inset depicts a Pd nanocube−PMMA sensor plate with a Pd nanocube loading of 0.03 wt %, dimensions of 6 mm × 12 mm and a thickness of 100 μm. (b) Sensor response expressed as [extinction@λ_1 − extinction@λ_2] for the Pd nanocube−PMMA nanocomposite, for neat Pd nanocubes drop-casted onto the fused silica support, and a melt-pressed neat PMMA control. The samples were exposed to five subsequent cycles of 10% H_2, five cycles of 0.5% CO, and five cycles of 10% H_2 + 0.5% CO, all in the synthetic air carrier gas. (c) Photograph of a 3D-printed Pd nanocube−PMMA composite sensor cap with a 0.02 wt % Pd loading plugged onto an SMA-905 multimode optical fiber. The nanocomposite material thickness at the tip of the cap is 200 μm. Inset: photograph of 3D-printed neat PMMA (white) and Pd nanocube−PMMA sensor caps (dark gray). (d) Fresh and 50 weeks aged 3D-printed Pd nanocube−PMMA and neat PMMA sensor cap response, defined as [extinction@λ_{max} − extinction@λ_{min}], to three subsequent cycles of 10% H_2, three cycles of 0.5% CO, and four cycles of 10% H_2 + 0.5% CO, all in the synthetic air carrier gas.

pressed sensor plate, the 3D-printed fiber cap sensor remained fully responsive even at severe CO poisoning conditions, thereby confirming the anticipated selective molecular sieving function of the PMMA matrix and the selective response of the Pd nanocubes to H_2 (Figure 5d, blue curve).[31] The 3D-printed neat PMMA control also in this case exhibited no response to any of the tested gases (Figure 5d, gray curve).

Finally, to test the long-term stability of our plasmonic plastic nanocomposite, we repeated the same experiment after aging of the 3D-printed sensor cap for 50 weeks at ambient conditions in air. Remarkably, the response to hydrogen, as well as the protection against deactivation by CO, is virtually unchanged (Figure 5d, red curve). This result thus advertises plasmonic plastic materials as an attractive solution for hydrogen sensors where frequent sensor recalibration due to aging and deactivation is one of the main limitations of existing commercial sensor solutions.

■ CONCLUSIONS

Plasmonic plastic nanocomposites provide a flexible material platform for melt-processed active plasmonic sensor devices, where functions like molecular sieving and ease of economic and scalable processing are intrinsically included. Furthermore,

the melt-processed plasmonic plastic nanocomposite-H_2 gas sensors we have presented challenge existing plasmonic H_2 sensor platforms, utilizing 2D arrays of nanofabricated or self-assembled nanoparticles on flat surfaces, since they are a conceptually fundamentally different paradigm for the scalable production of 3D devices. In our plasmonic plastic nanocomposite material, the plasmonically active and hydride-forming Pd nanocubes respond selectively to H_2 through a distinct change in their optical properties. At the same time, the PMMA matrix: (i) acts as a molecular sieve that prevents sensor deactivation by other molecular species, such as CO; (ii) is a means to stabilize the shape of the embedded nanocrystals; (iii) prevents their aggregation; and (iv) ensures sensor long-term stability, thereby drastically reducing the need for recalibration. This breakthrough was corroborated by the successful testing of melt-pressed and 3D-printed sensor plates and caps, respectively, that were directly integrated with a miniaturized optical sensor device prototype and with an off-the-shelf fiber-optic solution. These implementations were then successfully used to demonstrate H_2 detection in simulated application conditions in synthetic air with deactivating CO contamination, and revealed virtually unchanged sensor response and deactivation resistance even after 50 weeks of plasmonic plastic sensor aging at ambient conditions in air.

In a wider perspective, our work enables next-generation optical gas sensors centered on the idea of melt-processed plasmonic plastic nanocomposite materials that combine tailored plasmonic nanocrystal signal transducers with polymer matrix materials, selected and optimized based on the specific analyte to be detected. Furthermore, we envision the application of these materials in other branches of plasmonics, including magnetoplasmonics, plasmonic metamaterials, and plasmon-enhanced photovoltaics, where cost-effective scalable fabrication is critical for large-scale commercial integration in real devices and where the almost endless opportunities provided by combining polymer and colloidal chemistry will enable compelling opportunities in terms of rational material design and function.

■ METHODS

Nanoparticle Synthesis. The following chemicals were used: hexadecyltrimethylammonium bromide (CTAB, ≥98.0% Sigma-Aldrich), L-ascorbic acid (99% Sigma-Aldrich), sodium borohydride (≥98.0%), palladium(II) chloride (99% Sigma-Aldrich), and hydrochloric acid 37% (Sigma-Aldrich).

Pd nanocubes stabilized with CTAB were synthesized using a procedure reported elsewhere[32] with slight modifications where appropriate. A 10 mM H_2PdCl_4 solution was prepared by dissolving 0.1773 g $PdCl_2$ in 10 mL of 0.2 M HCl; thereafter, the solution was diluted up to 100 mL in Milli-Q H_2O (18.2 MΩ). H_2PdCl_4 (0.5 mL) was added to a 12.5 mM CTAB solution. The mixture was heated up to 95 °C, and 80 μL of 100 mM ascorbic acid was added under rapid stirring. Subsequently, the mixture was kept in the water bath for 30 min. Next, the reaction mixture was centrifuged at 8000 rpm, and the obtained pellet was dispersed in Milli-Q H_2O to obtain 4×10^{11} [NPs/mL]. To test the role of nanoparticle concentration in the nanocomposite in H_2 sensing, Pd nanocubes were also synthesized with the following concentrations: 1×10^{11}, 5×10^{11}, 1×10^{12}, 2×10^{12}, and 5×10^{12} [NPs/mL] by changing the volumes while maintaining the ratio and concentrations of the reactants.

Composite Compounding. Poly(methyl methacrylate), PMMA, powder with a weight-average molecular weight, M_w, of 75 000 g/mol, a polydispersity index, PDI, of 2.8 and a density of 1.2 g/cm³ was obtained from Polysciences Inc. The Pd−PMMA composite was prepared by pouring the aqueous Pd nanoparticle dispersions onto the PMMA powder, followed by drying at 80 °C overnight. The dry mixtures were compounded for 5 min in an Xplore Microcompounder MC5 at 200 °C, extruded through a 1.0 mm die, and collected onto a conveyor belt at slow speed, resulting in filaments with a diameter of 1.75 ± 0.1 mm.

Melt Pressing of Plates. Melt-pressed plates were produced with a hot press from AB Nike Hydralik, using extruded filaments as raw material. The Pd nanocube−PMMA samples were pressed at 200 °C and 5 tons for 3 min and then under 10 tons for 2 min, with metal spacers to control their final thickness ranging from 50 to 800 μm. For H_2 sensing with the prototype sensor device, 100 μm thick plates were melted onto a fused silica substrate for structural support.

3D Printing *via* Fused Filament Fabrication. For the fused filament fabrication of the Pd−PMMA composite, we used a Massportal Pharaoh XD printer. The printing was carried out at a nozzle temperature of 210 °C, with a build-plate temperature of 60 °C and a printing speed of 1000 mm/min.

Elemental Analysis. Elemental analysis for the Pd content in the composite was performed on samples dried at 60 °C for 4 h at MIKROLAB, Kolbe Germany.

Transmission Electron Microscopy. All nanoparticle and nanocomposite samples were imaged using a Tecnai T20 TEM microscope with a LaB6 gun, operating at 200 kV or a Titan 80−300 TEM microscope with a field emission gun, operating at 300 kV. The nanoparticle solution sample was prepared on a pure carbon 200 mesh copper grid, and Pd−PMMA nanocomposites were prepared on a Lacey 400 mesh copper grid.

UV−Vis Spectroscopy. The UV−visible absorbance spectra were obtained with a Cary 5000 spectrophotometer within the 350−800 nm spectral range.

Scanning Small-Angle X-ray Scattering (Scanning-SAXS). Scanning-SAXS measurements were carried out at the cSAXS beamline of the Swiss Light Source (SLS) at the Paul Scherrer Institute (PSI) in Villigen, Switzerland. The sample was scanned at an energy of 11.2 keV, and the beam size was 40 μm × 40 μm. The sample-to-detector distance was 2.16 m. A Pilatus 2 M detector was used to acquire small-angle scattering patterns. The step sizes used were 40 μm × 40 μm, while the applied exposure time was 0.2 s. Data processing was carried out using the "cSAXS scanning SAXS package" developed by the CXS group, Paul Scherrer Institute, Switzerland.[33] The size determination was performed using the SASView 4.2.0 software.

Hydrogen Sensing Experiments. The H_2 sensing experiments were carried out in (i) a vacuum chamber described in detail elsewhere[7,26] (Figure SI 9), (ii) a homebuilt flow reactor (Figure SI 10), and (iii) the hydrogen sensor prototype device. The measurements in the vacuum chamber and in the flow reactor were executed at 30 °C (the temperature was maintained by external heating), while those in the homebuilt flow reactor and the prototype sensor device were done at 21 °C (ambient temperature of the testing lab). We used multimode optical fibers and a spectrophotometer (Avantes SensLine AvaSpec-2048XL). In the flow reactor, the gas flow was regulated by mass flow controllers (Bronkhorst LowΔP). The total gas flow was 200 mL/min using synthetic air as the carrier gas. The 3D-printed fiber caps were mounted in a flow reactor equipped with a CF flange fiber-optic feed-through and a silica vacuum viewport connected to a light source (Avantes AvaLight-Hal Mini) and the spectrophotometer, respectively. The sensing was performed in transmission mode. The prototype sensor device is equipped with both an internal light source and a detector and operates in transmission mode. It was connected to the same set of mass flow controllers for the gas flow and composition regulation as the flow reactor.

■ ASSOCIATED CONTENT

ⓢ Supporting Information

The Supporting Information is available free of charge at https://pubs.acs.org/doi/10.1021/acsanm.0c01907.

Transmission electron microscopy of Pd nanocubes after synthesis and compounding; small-angle X-ray scattering for Pd nanocube–PMMA; Pd nanocube isotherm and response/recovery to/from a 750 mbar hydrogen pressure; raw data for the Arrhenius analysis of hydrogen sorption kinetics; calculation of the apparent activation energies of hydrogen sorption; raw data for the derivation of sorption-order parameter; modeling of hydrogen sorption kinetics of Pd nanocube–PMMA; hydrogen diffusion and permeability measurements on neat PMMA and Pd nanocube–PMMA plates; and hydrogen gas sensing test setups (PDF)

■ AUTHOR INFORMATION

Corresponding Authors

Kasper Moth-Poulsen − *Department of Chemistry and Chemical Engineering, Chalmers University of Technology, 412 96 Göteborg, Sweden;* orcid.org/0000-0003-4018-4927; Email: kasper.moth-poulsen@chalmers.se

Christian Müller − *Department of Chemistry and Chemical Engineering, Chalmers University of Technology, 412 96 Göteborg, Sweden;* orcid.org/0000-0001-7859-7909; Email: christian.muller@chalmers.se

Christoph Langhammer − *Department of Physics, Chalmers University of Technology, 412 96 Göteborg, Sweden;* orcid.org/0000-0003-2180-1379; Email: clangham@chalmers.se

Authors

Iwan Darmadi − *Department of Physics, Chalmers University of Technology, 412 96 Göteborg, Sweden;* orcid.org/0000-0002-5921-9336

Alicja Stolaś − *Department of Chemistry and Chemical Engineering, Chalmers University of Technology, 412 96 Göteborg, Sweden;* orcid.org/0000-0002-6736-9553

Ida Östergren − *Department of Chemistry and Chemical Engineering, Chalmers University of Technology, 412 96 Göteborg, Sweden*

Barbara Berke − *Department of Physics, Chalmers University of Technology, 412 96 Göteborg, Sweden;* orcid.org/0000-0002-3105-2036

Ferry Anggoro Ardy Nugroho − *Department of Physics, Chalmers University of Technology, 412 96 Göteborg, Sweden;* orcid.org/0000-0001-5571-0454

Matteo Minelli − *Department of Civil, Chemical, Environmental and Materials Engineering, University of Bologna, 40131 Bologna, Italy;* orcid.org/0000-0003-4662-1526

Sarah Lerch − *Department of Chemistry and Chemical Engineering, Chalmers University of Technology, 412 96 Göteborg, Sweden;* orcid.org/0000-0001-5968-8178

Irem Tanyeli − *Department of Physics, Chalmers University of Technology, 412 96 Göteborg, Sweden; Insplorion AB, 413 90 Göteborg, Sweden;* orcid.org/0000-0002-5433-2524

Anja Lund − *Department of Chemistry and Chemical Engineering, Chalmers University of Technology, 412 96 Göteborg, Sweden*

Olof Andersson − *Insplorion AB, 413 90 Göteborg, Sweden*

Vladimir P. Zhdanov − *Department of Physics, Chalmers University of Technology, 412 96 Göteborg, Sweden; Boreskov Institute of Catalysis, Russian Academy of Sciences, Novosibirsk 630090, Russia*

Marianne Liebi − *Department of Physics, Chalmers University of Technology, 412 96 Göteborg, Sweden;* orcid.org/0000-0002-5403-0593

Complete contact information is available at:
https://pubs.acs.org/10.1021/acsanm.0c01907

Author Contributions

#I.D., A.S., and I.Ö. contributed equally.

Author Contributions

I.D. executed and analyzed the H_2 sensing experiments and the optical characterization of the composite; participated in the composite material planning; made all figures; and assisted during the writing of the manuscript. A.S. synthesized all nanoparticles, executed TEM analysis, participated in the composite material planning, and assisted during the writing of the manuscript. I.Ö. compounded, melt-pressed, and 3D-printed all nanocomposite samples; executed the elemental analysis; participated in the composite material planning; and assisted during the writing of the manuscript. B.B. co-executed the scanning-SAXS measurements and the corresponding data analysis. F.A.A.N. participated in the planning, execution, and analysis of H_2 sensing experiments. M.M. executed the H_2 permeability measurements for the Pd nanocube–PMMA system and performed the corresponding data analysis. S.L. participated in the nanocrystal synthesis. I.T. executed the H_2 sensing experiments with the commercial device. A.L. assisted in the compounding and 3D printing of nanocomposites. O.A. performed the data analysis from the commercial device. V.P.Z. developed the diffusion front model and corresponding analysis. M.L. co-executed the scanning-SAXS measurements and assisted in the corresponding data analysis. K.M.-P. coordinated the nanoparticle synthesis part of the project. C.M. coordinated the nanocomposite compounding and 3D printing part of the project. C.L. coordinated the sensing part of the work, as well as the project as a whole, and wrote the manuscript.

Notes

The authors declare the following competing financial interest(s): C.L. is co-founder of Insplorion AB.

All experimental data within the article and its Supplementary Information are available from the corresponding authors upon reasonable request.

■ REFERENCES

(1) Anker, J. N.; Hall, W. P.; Lyandres, O.; Shah, N. C.; Zhao, J.; Van Duyne, R. P. Biosensing with Plasmonic Nanosensors. *Nat. Mater.* **2008**, *7*, 442−453.

(2) Larsson, E. M.; Langhammer, C.; Zorić, I.; Kasemo, B. Nanoplasmonic Probes of Catalytic Reactions. *Science* **2009**, *326*, 1091−1094.

(3) Syrenova, S.; Wadell, C.; Nugroho, F. A. A.; Gschneidtner, T. A.; Diaz Fernandez, Y. A.; Nalin, G.; Świtlik, D.; Westerlund, F.; Antosiewicz, T. J.; Zhdanov, V. P.; Moth-Poulsen, K.; Langhammer, C. Hydride Formation Thermodynamics and Hysteresis in Individual Pd Nanocrystals with Different Size and Shape. *Nat. Mater.* **2015**, *14*, 1236−1244.

(4) Mayer, K. M.; Hafner, J. H. Localized Surface Plasmon Resonance Sensors. *Chem. Rev.* **2011**, *111*, 3828−3857.

(5) Tittl, A.; Giessen, H.; Liu, N. Plasmonic Gas and Chemical Sensing. *Nanophotonics* **2014**, *3*, 157−180.

(6) Wadell, C.; Syrenova, S.; Langhammer, C. Plasmonic Hydrogen Sensing with Nanostructured Metal Hydrides. *ACS Nano* **2014**, *8*, 11925−11940.

(7) Nugroho, F. A. A.; Darmadi, I.; Cusinato, L.; Susarrey-Arce, A.; Schreuders, H.; Bannenberg, L. J.; da Silva Fanta, A. B.; Kadkhodazadeh, S.; Wagner, J. B.; Antosiewicz, T. J.; Hellman, A.; Zhdanov, V. P.; Dam, B.; Langhammer, C. Metal−Polymer Hybrid Nanomaterials for Plasmonic Ultrafast Hydrogen Detection. *Nat. Mater.* **2019**, *18*, 489−495.

(8) Hydrogen to the Rescue. *Nat. Mater.* **2018**, *17* 565. DOI: 10.1038/s41563-018-0129-y.

(9) Adams, B. D.; Chen, A. The Role of Palladium in a Hydrogen Economy. *Mater. Today* **2011**, *14*, 282−289.

(10) Poyli, M. A.; Silkin, V. M.; Chernov, I. P.; Echenique, P. M.; Muiño, R. D.; Aizpurua, J. Multiscale Theoretical Modeling of Plasmonic Sensing of Hydrogen Uptake in Palladium Nanodisks. *J. Phys. Chem. Lett.* **2012**, *3*, 2556−2561.

(11) Xia, Y.; Xiong, Y.; Lim, B.; Skrabalak, S. E. Shape-Controlled Synthesis of Metal Nanocrystals: Simple Chemistry Meets Complex Physics? *Angew. Chem., Int. Ed.* **2009**, *48*, 60−103.

(12) Kalanur, S. S.; Lee, Y.-A.; Seo, H. Eye-Readable Gasochromic and Optical Hydrogen Gas Sensor Based on CuS−Pd. *RSC Adv.* **2015**, *5*, 9028−9034.

(13) Jiang, R.; Qin, F.; Ruan, Q.; Wang, J.; Jin, C. Ultrasensitive Plasmonic Response of Bimetallic Au/Pd Nanostructures to Hydrogen. *Adv. Funct. Mater.* **2014**, *24*, 7328−7337.

(14) Sacanna, S.; Korpics, M.; Rodriguez, K.; Colón-Meléndez, L.; Kim, S.-H.; Pine, D. J.; Yi, G.-R. Shaping Colloids for Self-Assembly. *Nat. Commun.* **2013**, *4*, No. 1688.

(15) Diaz Fernandez, Y. A.; Gschneidtner, T. A.; Wadell, C.; Fornander, L. H.; Lara Avila, S.; Langhammer, C.; Westerlund, F.; Moth-Poulsen, K. The Conquest of Middle-Earth: Combining Top-down and Bottom-up Nanofabrication for Constructing Nanoparticle Based Devices. *Nanoscale* **2014**, *6*, 14605−14616.

(16) Zhang, J.; Li, Y.; Zhang, X.; Yang, B. Colloidal Self-Assembly Meets Nanofabrication: From Two-Dimensional Colloidal Crystals to Nanostructure Arrays. *Adv. Mater.* **2010**, *22*, 4249−4269.

(17) Darmadi, I.; Nugroho, F. A. A.; Kadkhodazadeh, S.; Wagner, J. B.; Langhammer, C. Rationally Designed PdAuCu Ternary Alloy Nanoparticles for Intrinsically Deactivation-Resistant Ultrafast Plasmonic Hydrogen Sensing. *ACS Sens.* **2019**, *4*, 1424−1432.

(18) Palmisano, V.; Weidner, E.; Boon-Brett, L.; Bonato, C.; Harskamp, F.; Moretto, P.; Post, M. B.; Burgess, R.; Rivkin, C.; Buttner, W. J. Selectivity and Resistance to Poisons of Commercial Hydrogen Sensors. *Int. J. Hydrogen Energy* **2015**, *40*, 11740−11747.

(19) Clerbaux, C.; Edwards, D. P.; Deeter, M.; Emmons, L.; Lamarque, J. F.; Tie, X. X.; Massie, S. T.; Gille, J. Carbon Monoxide Pollution from Cities and Urban Areas Observed by the Terra/MOPITT Mission. *Geophys. Res. Lett.* **2008**, *35*, No. L03817.

(20) Hong, J.; Lee, S.; Seo, J.; Pyo, S.; Kim, J.; Lee, T. A Highly Sensitive Hydrogen Sensor with Gas Selectivity Using a PMMA Membrane-Coated Pd Nanoparticle/Single-Layer Graphene Hybrid. *ACS Appl. Mater. Interfaces* **2015**, *7*, 3554−3561.

(21) Whitelam, S.; Hedges, L. O.; Urban, J. J.; Pint, C. L.; Javey, A.; Bardhan, R. Uncovering the Intrinsic Size Dependence of Hydriding Phase Transformations in Nanocrystals. *Nat. Mater.* **2013**, *12*, 905−912.

(22) Baldi, A.; Narayan, T. C.; Koh, A. L.; Dionne, J. A. In Situ Detection of Hydrogen-Induced Phase Transitions in Individual Palladium Nanocrystals. *Nat. Mater.* **2014**, *13*, 1143−1148.

(23) Jeon, K. J.; Moon, H. R.; Ruminski, A. M.; Jiang, B.; Kisielowski, C.; Bardhan, R.; Urban, J. J. Air-Stable Magnesium Nanocomposites Provide Rapid and High-Capacity Hydrogen Storage without Using Heavy-Metal Catalysts. *Nat. Mater.* **2011**, *10*, 286−290.

(24) Langhammer, C.; Kasemo, B.; Zorić, I. Absorption and Scattering of Light by Pt, Pd, Ag, and Au Nanodisks: Absolute Cross Sections and Branching Ratios. *J. Chem. Phys.* **2007**, *126*, No. 194702.

(25) Zorić, I.; Zäch, M.; Kasemo, B.; Langhammer, C. Gold, Platinum, and Aluminum Nanodisk Plasmons: Material Independence, Subradiance, and Damping Mechanisms. *ACS Nano* **2011**, *5*, 2535−2546.

(26) Wadell, C.; Nugroho, F. A. A.; Lidström, E.; Iandolo, B.; Wagner, J. B.; Langhammer, C. Hysteresis-Free Nanoplasmonic Pd-Au Alloy Hydrogen Sensors. *Nano Lett.* **2015**, *15*, 3563−3570.

(27) Chen, P.; Tran, N. T.; Wen, X.; Xiong, Q.; Liedberg, B. Inflection Point of the Localized Surface Plasmon Resonance Peak: A General Method to Improve the Sensitivity. *ACS Sens.* **2017**, *2*, 235−242.

(28) Langhammer, C.; Zorić, I.; Larsson, E. M.; Kasemo, B. Localized Surface Plasmons Shed Light on Nanoscale Metal Hydrides. *Adv. Mater.* **2010**, *22*, 4628−4633.

(29) Nugroho, F. A. A.; Darmadi, I.; Zhdanov, V. P.; Langhammer, C. Universal Scaling and Design Rules of Hydrogen-Induced Optical Properties in Pd and Pd-Alloy Nanoparticles. *ACS Nano* **2018**, *12*, 9903−9912.

(30) Grönbeck, H.; Zhdanov, V. P. Effect of Lattice Strain on Hydrogen Diffusion in Pd: A Density Functional Theory Study. *Phys. Rev. B* **2011**, *84*, No. 052301.

(31) Minelli, M.; Sarti, G. C. Elementary Prediction of Gas Permeability in Glassy Polymers. *J. Membr. Sci.* **2017**, *521*, 73−83.

(32) Niu, W.; Li, Z. Y.; Shi, L.; Liu, X.; Li, H.; Han, S.; Chen, J.; Xu, G. Seed-Mediated Growth of Nearly Monodisperse Palladium Nanocubes with Controllable Sizes. *Cryst. Growth Des.* **2008**, *8*, 4440−4444.

(33) Bunk, O.; Bech, M.; Jensen, T. H.; Feidenhans'L, R.; Binderup, T.; Menzel, A.; Pfeiffer, F. Multimodal X-Ray Scatter Imaging. *New J. Phys.* **2009**, *11*, No. 123016.